Potential-Dependent Restructuring and Chemical Noise at Au–Ag–Au Atomic Scale Junctions

Tai-Wei Hwang[†] and Paul W. Bohn[†,‡,*]

[†]Department of Chemical and Biomolecular Engineering, University of Notre Dame, Notre Dame, Indiana 46556, United States and [‡]Department of Chemistry and Biochemistry, University of Notre Dame, Notre Dame, Indiana 46556, United States

ABSTRACT The effect of electrochemical potential on the behavior of electrochemically deposited Au–Ag–Au bimetallic atomic scale junctions (ASJs) is addressed here. A common strategy for ASJ production begins with overgrown nanojunctions and uses electromigration to back-thin the junction. Here, these steps are carried out with the entire junction under electrochemical potential control, and the relationship between junction stability and applied potential is characterized. The control of electrochemical potential provides a reliable method of regulating the size of nanojunctions. In general, more anodic potentials decrease junction stability and increase the rate at which conductance decays. Conductance behavior under these labile conditions is principally determined by Ag oxidation potential, electrochemical potential-induced surface stress, and the nature of the adsorbate. Junctions fabricated at more cathodic potentials experience only slight changes in conductance, likely due to surface atom diffusion and stress-induced structural rearrangement. Electrochemical potential also plays a significant role in determining adsorption–desorption kinetics of surface pyridine at steady state at Au–Ag–Au ASJs, as revealed through fluctuation spectroscopy. Average cutoff frequencies increase at more anodic potentials, as does the width of the cutoff frequency distribution measured over 80 independent runs. Three reversible reactions—pyridine adsorption, Ag atom desorption, and Ag-pyridine complex dissolution—can occur on the surface, and the combination of the three can explain the observed results.

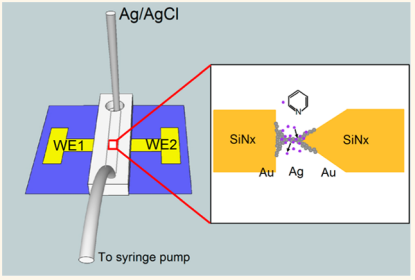

KEYWORDS: atomic scale junctions · nanowire · electrochemical potential · fluctuation spectroscopy · pyridine · adsorption kinetics

Atomic scale junctions (ASJs) have been studied for the past two decades, because they exhibit interesting quantum phenomena applicable to fundamental studies of nanoelectronics,[1–4] and as the limiting case of nanostructures, they possess the maximum possible surface-to-volume ratio, making them interesting for applications in chemical sensing.[5–7] A number of metals have been used to fabricate ASJs, with metals from different groups showing different conductance behaviors. For example, noble metals (Au, Ag, Cu) exhibit conductance peaks at multiples of G_0 ($G_0 = 2e^2/h = 77.4\ \mu S = 1/(12.9\ k\Omega)$ is the conductance quantum) at low temperature, while transition metals (Pd, Pt, Nb) show a single broad peak in the range $1.5\ G_0 \leq G \leq 2.5\ G_0$.[8] Typically ASJs are fabricated by one of two principal approaches: mechanical formation and electrochemical deposition. Mechanical formation, including mechanically controllable break junctions[9] and the use of a scanning tunneling microscope (STM),[10] provides rapid, repeatable junction formation that allows the ASJs to be characterized statistically over thousands of short lifetime conductance traces. Electrochemical deposition and dissolution, despite being more complicated, can yield junctions with lifetimes from several minutes to hours, thereby enabling detailed fundamental studies and opening the door to applications,[11–14] including metal nanofilament devices, which are the basis of resistive random access memories, neuromorphic architectures based on resistive switching,[15–19] and current-driven single-atom switches.[20]

Common electrochemical approaches to ASJ fabrication maintain a well-defined potential between two ends of a nanogap (for electrodeposition) or a nanowire (for electrodissolution), but the potential is frequently not defined with respect to a well-defined reference electrode, such as

* Address correspondence to pbohn@nd.edu.

Received for review November 26, 2013 and accepted January 13, 2014.

Published online January 13, 2014
10.1021/nn406098u

Ag/AgCl. Thus, the potential offset between the electrodes is well-defined, but the absolute potential is determined by the nature of the surface and the solution. The effect of maintaining a well-defined electrochemical reference potential on previously prepared ASJs has been studied using both mechanically and electrochemically fabricated ASJs. For example, Tao and co-workers created Au ASJs using a scanning tunneling microscope in an electrochemical cell and studied conductance behavior at different applied electrochemical potentials. They found that fractional conductance peaks appear at more cathodic potentials, and they attributed these to potential-induced defect scattering and a Fermi level shift.[21] Murakoshi and co-workers later explained the fractional conductance states with a hydrogen-incorporation model, citing a reduction in the density of states at the Fermi level of metals at the potential of hydrogen evolution that results in decreased conductance.[22−24] Tao and co-workers also introduced ac electrochemical potential modulation and demonstrated conductance changes due to modulation amplitude and electrolyte selection.[25] Controlling the electrochemical potential has also been used to increase the stability and lifetime of ASJs.[26,27] Moreover using the reference electrode as a gate electrode and switching its potential between on/off potentials allows the junction to be reversibly broken and regrown, thus realizing a switchable atomic scale transistor.[28]

ASJ surfaces also present a rich array of adsorption/desorption behavior. For example, molecular adsorption leads to conductance changes, providing a mechanism for chemical sensing.[6] Tao and co-workers worked with Cu ASJs and showed that the adsorbate-induced conductance change, ΔG, strongly depends on the size of the junction and the binding strength of the molecules: ΔG is larger for smaller junctions and stronger binding molecules.[7] Study of the magnitude of ΔG as a function of junction size has also been carried out in our laboratory using alkanethiols on Au ASJs. For junctions displaying $G > 20\ G_0$, the magnitude of ΔG is independent of junction conductance, similar to the behavior of boundary layer scattering on thin films;[29] for junctions below 20 G_0, sensitivity increases dramatically as conductance decreases, and impedance changes of 70% have been observed for monolayer adsorption on ASJs of 2−3 G_0.[6] In addition to causing conductance changes, molecular adsorption can also promote mechanical stability of ASJs. For example, Au ASJs created by STM in the presence of adenine can be elongated 3−4 times longer before conductance decreases compared to the case without adenine.[30] Cu ASJs show a larger conductance peak around 1 G_0 with addition of thiourea solution,[31] and with the protection of cyclodextrin the lifetime of Cu ASJs can be greatly prolonged.[32]

Recently, an electrochemical fabrication protocol was developed in our lab to reproducibly generate bimetallic Au−Ag−Au ASJs in high yield. The procedure starts by forming an overgrown ($G \gg 1\ G_0$) Ag nanojunction across a Au nanogap electrode followed by back-thinning the junction to atomic size, while monitoring the conductance *in situ*. Two approaches to junction thinning were reported. First, the electroplating solution is prepared with a chemical potential, *e.g.*, a low background concentration of Ag^+ for thinning a Ag nanowire, that allows the dissolution reaction to proceed with controlled kinetics.[33] However, size control remains difficult, and small conductance ASJs frequently do not survive switching out the electroplating solution to adsorbate solution, *e.g.*, pyridine in 1:1 MeOH−H_2O. In the second approach, adsorbate solution is delivered immediately after formation of the overgrown junction. Back-thinning is then accomplished *via* electromigration by adjusting the current.[34] This approach reproducibly yields Au−Ag−Au bimetallic ASJs that have been successfully used to detect the chemical noise produced by the equilibrium adsorption/desorption of the surface adsorbate (pyridine).

The aim of this work is to explore the relationship between electrochemical potential (ECP) and the resulting dynamics, including spontaneous restructuring events and adsorbate fluctuations that lead to chemical noise. First, the stability of overgrown nanojunctions under ECP control is characterized, principally through the conductance behavior displayed by Au−Ag−Au ASJs in response to the change of ECP. These results demonstrate a third thinning method in which adjusting the ECP leads to controllable thinning of overgrown junctions. Subsequent experiments target the measurement of pyridine adsorption/desorption from ASJ surfaces under ECP control using fluctuation spectroscopy. These experiments demonstrate that ECP control results in unusual trends in the characteristic cutoff frequency of the chemical noise that suggest complicated kinetics on the ASJ surface. The observed behavior is consistent with multiple reversible surface reactions occurring simultaneously.

RESULTS AND DISCUSSION

Dynamics of Ag Junctions under Electrochemical Potential Control. The overall architecture of the devices used in these studies is illustrated in Figure 1. Prior to studying junctions at atomic size, overgrown nanojunctions were first examined to define the range of potentials over which ASJs are stable. The preparation of overgrown junctions has been described previously.[33,34] As shown in Figure 1b and c, two Au electrodes in a tip and anvil configuration with nanometer scale gap ~100 nm, in Figure 1c, are defined by focused ion beam (FIB) milling. Applying a potential across the tip−anvil gap generates a concentrated electric field that directs Ag deposition from 10 μM Ag_2SO_4 + 0.1 M K_2SO_4 to be highly directional. ASJ growth under these conditions typically produces junctions with G in the

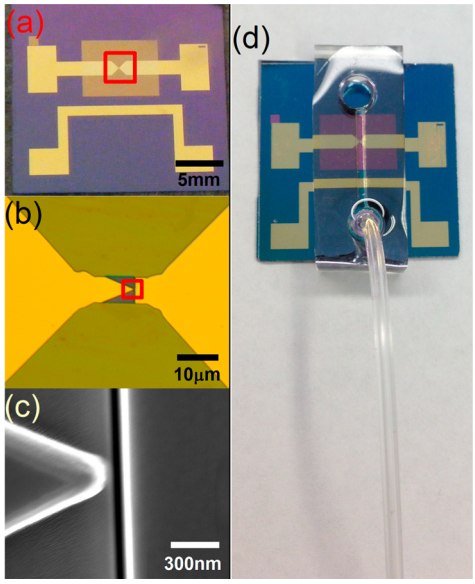

Figure 1. (a) Top view of the sample template. The highlighted area shows the nanogap electrodes prepared from a Au microbridge using focused ion beam milling. The bottom electrode is not used in this work. (b) Optical micrograph showing the microbridge after milling to produce the initial tip and anvil nanogap design. (c) Scanning electron micrograph (SEM) of the highlighted area in (b). (d) Photograph of the assembled device with microfluidic reagent delivery to the nanogap. Sample is coupled to the PDMS microfluidic channel; bottom tubing connects to a syringe pump; a Ag/AgCl reference electrode (not shown) is placed in the top open reservoir.

range 30−100 G_0, *i.e.*, an overgrown junction. Then the electroplating solution is immediately switched to electrolyte-free pyridine solution, *e.g.*, 1 mM pyridine in 1:1 (v:v) water−methanol (H_2O−MeOH), to chemically stabilize the junction against spontaneous dissolution.

Normal potentiostats do not function to apply potentials to two working electrodes (WEs) while measuring the current flowing between them, so an unconventional electronic setup was used to conduct experiments with the junction under ECP control; see Figure 2. A Ag/AgCl reference electrode was held at the virtual ground of the data acquisition card that served as a low-noise voltage source, and potentials (E_1, E_2) *vs* ground Ag/AgCl were applied to the sample across a series combination formed by an adjustable external ballast resistor, R_d, and the sample, R_s. In this setup, the Ag/AgCl electrode serves as both counter (CE) and reference (RE) electrode. Because the faradaic currents are limited by the ASJ size, they are very small, so the drift of the reference potential is negligible. Sample conductance was then acquired by measuring the voltage across the adjustable resistor, V_d. For experiments on junction stability under ECP control, $\Delta E = E_2 - E_1$ was fixed at 0.2 V, and R_d was set at 4 kΩ to minimize current-induced electromigration in the junctions. The combination of constant offset and changing E_1 naturally produces a potential gradient

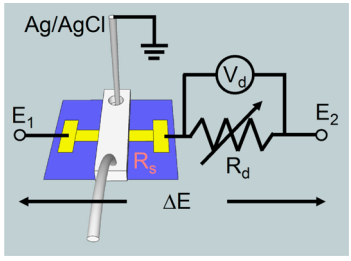

Figure 2. Schematic diagram showing the experimental configuration for conductance experiments at Au−Ag−Au bimetallic ASJs under electrochemical potential control. A data acquisition (DAQ) card is used to supply potentials E_1 and E_2 and to measure the voltage drop, V_d, across an adjustable external ballast resistor, R_d. The Ag/AgCl reference electrode is connected to the virtual ground of the DAQ card.

across the junction, $E(x)$, where all points are referenced to the Ag/AgCl RE/CE.

Figure 3 shows three typical conductance trajectories for overgrown Ag nanojunctions in response to the application of increasingly anodic ECP. All three figures illustrate that at sufficiently cathodic potential the junctions are stable indefinitely (hours). Also in all three cases an applied potential, E_1, is reached where the conductance begins to decrease in steps. In Figure 3a, the junction undergoes a small step-decrease in conductance at $E_1 = +0.3$ V, then spontaneously breaks when E_1 is increased to +0.4 V. Figure 3b illustrates a junction that decays with a much richer array of metastable intermediate conductance states at $E_1 = +0.2$, 0.3, 0.4, and 0.5 V. The conductance trajectory in Figure 3c is similar at more cathodic applied potentials, but the conductance drops in much smaller increments starting at $E_1 = +0.4$ V until it spontaneously breaks at $E_1 = +0.7$ V.

To investigate the effect of adsorbate concentration in determining the ECP-controlled thinning behavior, overgrown junctions immersed in 1 μM pyridine in 1:1 MeOH−H_2O were tested. The pyridine−Ag adsorption isotherm measured by surface-enhanced Raman scattering shows that 1 μM is below the linear region of the isotherm, while at 1 mM the surface coverage is saturated.[35] Figure 4 shows the conductance traces of junctions in 1 μM pyridine under ECP control. There are clear differences compared to the behavior of junctions studied in 1 mM pyridine. These junctions spontaneously break at more cathodic potentials, *e.g.*, at $E_1 = +0.1$ V in Figure 4a, a relatively low value compared to the behavior in 1 mM pyridine. The potential at which the junction spontaneously breaks can be positively shifted, for example by repeatedly forming and breaking the junction, but the spontaneous-break potential never exceeds +0.5 V in 1 μM pyridine. Comparison of ECP conductance trajectories at 1 μM and 1 mM clearly show that the degree of protection against spontaneous thinning/breaking is concentration dependent.

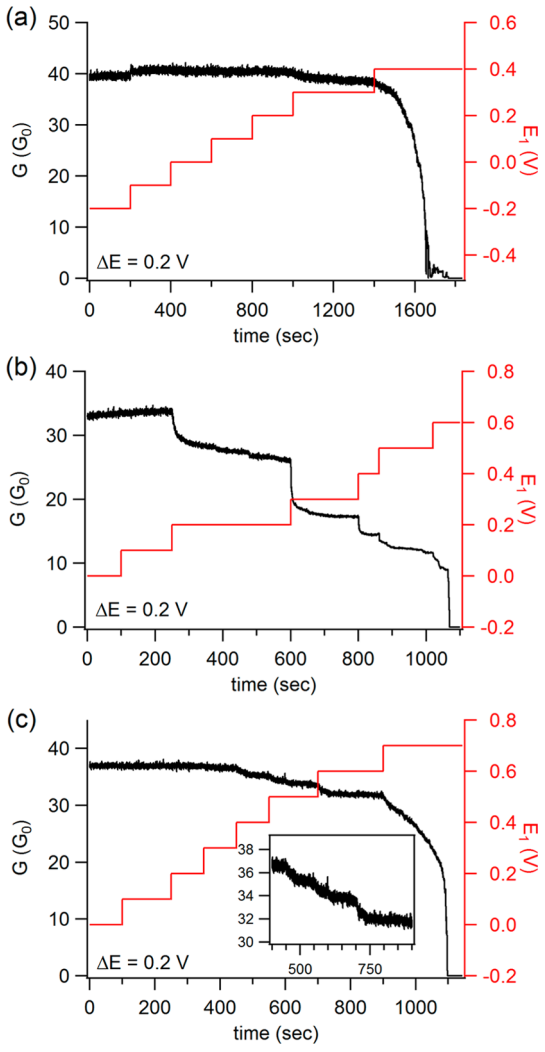

Figure 3. Conductance trajectories for overgrown Ag junctions in response to application of increasingly anodic potentials in 1 mM pyridine in 1:1 MeOH−H_2O. In each panel conductance (black) is plotted on the left axis, and applied potential (red) is plotted on the right axis. Conductance trajectories in (a)−(c) are obtained as a function of potential at E_1, but all trajectories are obtained at the same ΔE = 0.2 V *vs* Ag/AgCl. (Inset, c) Magnified view of the conductance behavior from 400 to 900 s.

Three important factors should affect junction stability. First, Ag oxidizes and dissolves as $Ag^+_{(aq)}$ at anodic potentials (E^0 for Ag/Ag^+ is +0.577 V *vs* Ag/AgCl). The conductance of junctions studied here begins to drop at potentials lower than $E^0(Ag/Ag^+)$, consistent with spontaneous, potential-dependent restructuring of the pyridine-decorated Ag ASJs in 1:1 MeOH−H_2O. The measured conductance reflects the total current flowing in the junction, which in turn is composed of both faradaic and in-wire components, *i.e.*, $i_{total} = i_{farad} + i_{wire}$. However, any faradaic contribution must occur when the conductance is changing and the ASJ is reconfiguring. Once the junction stabilizes at a metastable configuration, positive and negative contributions to i_{farad} cancel, and all of the current must arise from the potential difference across the

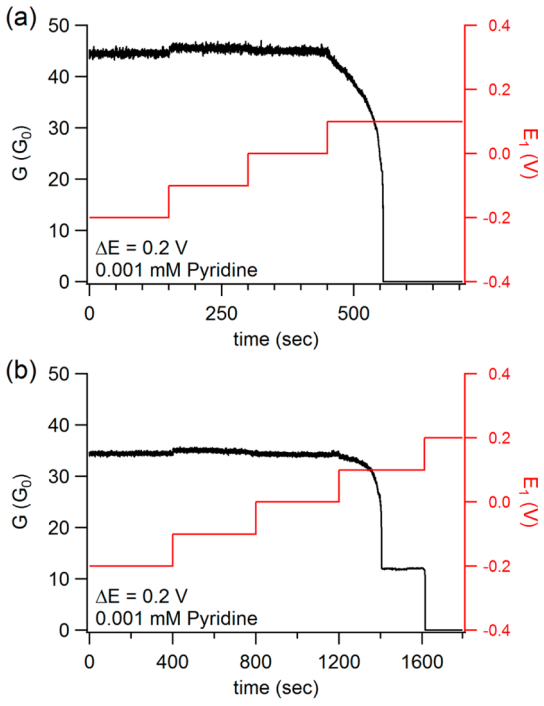

Figure 4. Conductance trajectories for overgrown Ag junctions in response to application of increasingly anodic potentials in 1 μM pyridine in 1:1 MeOH−H_2O. In each panel conductance (black) is plotted on the left axis, and applied potential (red) is plotted on the right axis. Conductance trajectories in (a) and (b) are obtained as a function of potential at E_1, but all trajectories are obtained at the same ΔE = 0.2 V *vs* Ag/AgCl.

junction, ΔE, and $i_{total} \approx i_{wire}$. Thus, the absence of supporting electrolyte, which would normally result in a significant *iR* drop between the ASJ WE and the Ag/AgCl RE, is not relevant, because the net i_{farad} is negligible under these circumstances.

Plieth[36] predicted a negative shift in the redox potential in a small metal particle, E^0_p, given by

$$E_p{}^0 = \left(E_{bulk}{}^0 - \frac{2\gamma v_M}{zFr}\right) \quad (1)$$

where γ is the surface tension, v_M is the molar volume, z is the lowest valence state, F is Faraday's constant, and r is the nanoparticle radius. These size-dependent potential shifts were used to explain the mechanism of electrochemical Ostwald ripening of Ag particles as arising from differences in the equilibrium Ag^+ concentration around each particle, thus resulting in size evolution.[37] Ivanova *et al.* empirically examined the oxidation potential of silver nanoparticles and showed that the size dependent E^0_p shift agrees with theory.[38] Ag junctions with $G \approx 10-100\ G_0$ are nanoscale, so the redox potential should be shifted cathodically from the standard value for bulk Ag, consistent with the conductance trajectories in Figure 3.

Another factor that could affect junction stability is the electrochemical potential-induced surface stress in the double-layer charging regime. Surface stress is

relevant, because it is known to be related to surface reconstruction,[39,40] and in the limit of an ASJ, the entire junction is surface or near-surface. Abrupt conductance changes have been observed during the application of large potentials in nanowires,[41] and these have been correlated with atomic configuration rearrangements.[42] Therefore, part of the behavior of Figure 3 could be due to ECP-induced surface stress that causes the deformation. Yet, this cannot fully explain why junctions stabilize after deformation or why the degree of deformation varies so widely, *cf.* Figure 3b and c.

The third important factor is the adsorbate (pyridine). The effects of pyridine adsorption on ASJ conductance have been studied previously,[34] the principal result being that pyridine can stabilize Ag ASJs in 1:1 H_2O−MeOH, even though it is a somewhat unstable environment for bare Ag. Pyridine−Ag ASJs exhibit complex restructuring behavior; when the ASJ is initially exposed to pyridine, it adsorbs to the Ag surface and lowers the surface energy. However, even at full coverage, adsorbate-induced surface restructuring occurs over periods of minutes.[43] Thus, Ag ASJs can be restructured to more stable states after longer adsorption time, and the time between pyridine exposure and conducting the ECP-conductance experiment is likely important in determining the detailed dynamical behavior observed. For example, junctions exposed to pyridine for longer periods typically exhibit a larger number of smaller conductance steps, such as those observed in Figure 3c, while behavior similar to that in Figure 3b is observed if the conductance measurement is carried out soon after pyridine solution is introduced.

Relation of ECP-Induced Thinning and Electromigration. In order to assess the relative contributions of ECP and electromigration to the stability of overgrown junctions, an experiment was performed in which the RE was removed. Figure 5 shows an ECP-conductance trajectory in 1 μM pyridine. During the thinning process, at $t \approx 2350$ s, the RE was removed from the system. Prior to removal of the RE, the junction was observed to undergo spontaneous restructuring accompanied by decreased conductance at $E_1 = +0.3$ V. However, after the RE was removed, the ASJ conductance stopped decreasing and remained stable at ~9 G_0 for an extended period; see Figure 5, inset. Since the in-wire potential remained unchanged at $\Delta E = +0.2$ V, and since the wire potential would be expected to float to a value determined by the solution and wire conditions after removing the RE, the result suggests that ECP is more important than electromigration in determining junction stability under these conditions.

Poising the ASJ at sufficiently anodic potentials clearly causes overgrown Au−Ag−Au ASJs to undergo structural reorganization accompanied by decreased conductance, but the question arises whether this

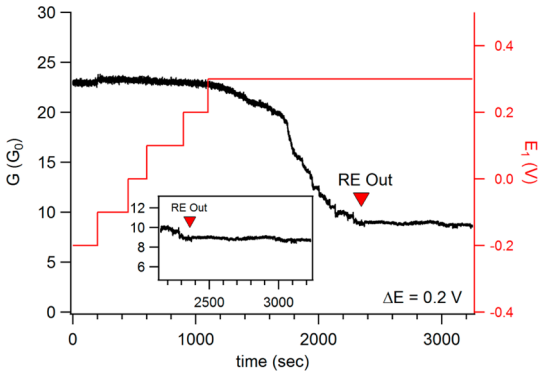

Figure 5. Conductance trajectory for an overgrown Ag junction in response to application of increasingly anodic potentials in 1 μM pyridine in 1:1 MeOH−H_2O, showing the effect of removing the RE at $t \approx 2350$ s. (Inset) Magnified view of the conductance from 2200 to 3200 s.

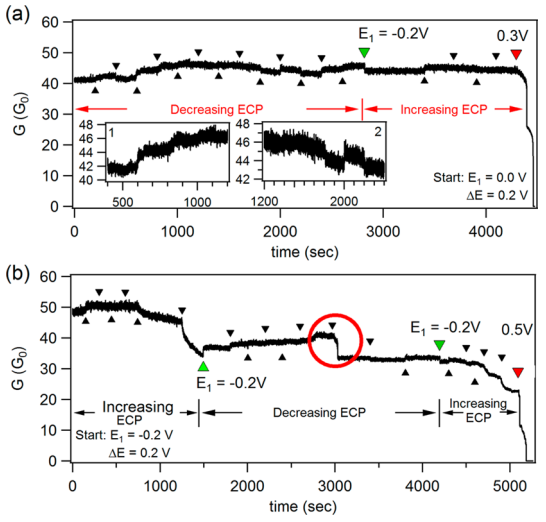

Figure 6. Conductance trajectories for overgrown Ag junctions in response to application of increasingly anodic or cathodic potentials in 1 mM pyridine in 1:1 MeOH−H_2O. (a) Initially decreasing potentials starting at $E_1(t_0) = 0.0$ V. Each marker represents a ±0.1 V change in the indicated direction. Green arrow: potential reset to $E_1 = -0.2$ V. Red arrow: onset of spontaneous breaking. (Insets) Magnified view of conductance in the early stages of increasing (1) or decreasing (2) junction size within the decreasing ECP time window. (b) Initially increasing potentials starting at $E_1(t_0) = -0.2$ V. Each marker represents a ±0.1 V change in the indicated direction. Green arrows: potential reset to $E_1 = -0.2$ V. Red arrow: onset of spontaneous breaking.

behavior is reversible and whether increasingly cathodic potentials result in growth of the junction. Figure 6 shows the results of a series of experiments in which ECP control is applied to Au−Ag−Au ASJs in 1 mM pyridine, with both increasing and decreasing potentials. In Figure 6, each triangular marker represents a 0.1 V step change in potential in the indicated direction (increasing = more anodic, decreasing = more cathodic). Starting with Figure 6a, the potential is initially poised at $E_1 = 0.0$ V and stepped to increasingly cathodic values. Although the value of the conductance varies somewhat, the Ag junction is clearly stable

at all of these applied potentials. Interestingly, as shown in inset 1, ASJ conductance increases slightly even in the absence of solution Ag^+. This behavior could result from either Ag cluster dissolution and subsequent redeposition or reductive ECP changing the surface energy so that Ag atoms migrate along the surface, producing a somewhat thicker ASJ. Both mechanisms are consistent with reports that show ECPs enabling altered morphology and islanding on metallic surfaces.[44,45] At $t \approx 2800$s, E_1 is switched from -1.3 V to -0.2 V followed by an increasingly anodic potential program, until the junction spontaneously breaks when the potential reaches $+0.3$ V.

Figure 6b shows the results of an experiment in which ECP was controlled in three stages. Starting from $E_1 = -0.2$ V, the ECP is increased in 0.1 V steps, and the conductance is stable until $E_1 = +0.4$ V, at which point a spontaneous restructuring to a new state begins. Then, E_1 is switched from $+0.4$ V to -0.2 V, which immediately stabilizes the junction. Next the ECP is decreased in 0.1 V steps, and the conductance response is similar to that observed in Figure 6a, except for the anomalous event at $E_1 = -0.8$ V (circled in red). Events like this are observed periodically and are likely due to junction reconstruction caused by ECP-induced stress. Finally, the potential is flipped again to $E_1 = -0.2$ V and is then increased in 0.1 V steps. The conductance starts to decrease at $+0.2$ V and then spontaneously breaks at $+0.5$ V.

The ASJs are clearly labile and can be induced to exhibit slow increases in conductance or sudden decreases, as seen above. It is evident that ECP strongly influences the stability of Ag ASJs, and the conductance behavior is consistent in showing either a slight increase in conductance, in response to cathodic excursions, or step-decreases in conductance at anodic ECPs. Thus, ECP-controlled thinning of overgrown nanojunctions provides a ready method to control the size and conductance of atomic scale metal junctions.

Adsorption/Desorption Dynamics on Ag ASJs under ECP Control. The physical size of ASJs minimizes the population of adsorbed molecules, but it also enhances the electrical signal (impedance change) associated with molecular adsorption. This makes ASJs good candidates not only for chemical sensors but also to study fundamental details of surface processes, such as the chemical noise stemming from fluctuations in adsorbate population. We recently reported using fluctuation spectroscopy to study the chemical noise generated by pyridine adsorption−desorption on Ag ASJs,[34] and here we extend these studies to ASJs under potential control.

In general, the main noise components in an electrical circuit containing an ASJ are $1/f$ ($1/f^{\alpha}$) noise dominating the low-frequency range and Johnson−Nyquist noise from diffusive processes at higher frequencies. In addition, if the adsorbate population, N, affects electron scattering in the ASJ, as is the case for Lewis bases,[6,29] the fluctuations in this population, δN, can give rise to a chemically derived noise component that can exceed the $1/f$ noise at higher frequencies. For the circuit in Figure 2, the chemical noise signal, δV_{dl}, is proportional to the chemically induced resistance fluctuation, δR_{dl}, and can be expressed by

$$\delta V_{dl} = \frac{R_d \Delta E}{(R_s + R_d)^2} \delta R_{dl} \quad (2)$$

Based on the work of Feher and Weissman,[46] the power spectral density (PSD) of population fluctuations, δN, at equilibrium in a reversible system is a Lorentzian function given by

$$\langle \delta N(f)^2 \rangle = \frac{4\tau \left\langle N\left(1 - \frac{\langle N \rangle}{N_T}\right)\right\rangle}{1 + (2\pi f \tau)^2} \quad (3)$$

where N_T is the total population, containing N molecules of the species of interest, and τ is the relaxation time. Equations 2 and 3 can be connected through,

$$\delta R_{dl} = \left(\frac{\partial R}{\partial N}\right) \delta N \quad (4)$$

Since each molecule contributes equally to a resistance change, $(\partial R/\partial N)$ is constant,[29] and δV_{dl} is linearly related to δN. As a result, the PSD of the chemical noise is a Lorentzian with characteristic cutoff frequency $f_c = (2\pi\tau)^{-1}$.

Chemical noise was sufficiently large to be measurable only over certain combinations of (E_1, ΔE). For example, for ASJs with conductance $G < 5\ G_0$, distinguishable Lorentzian components could be obtained for $\Delta E = +0.4$ V and $R_d = 4$ kΩ. Figure 7 shows an example of a typical PSD obtained by sequentially autocorrelating and Fourier transforming the current, as measured by V_d in Figure 2. When added to $1/f$ noise, Lorentzian chemical noise components alter the $1/f$ slope, producing an inflection point that indicates f_c. Detailed, statistically robust procedures for finding f_c, including the curve fitting and data development, have been published previously.[34]

The junction stability experiments discussed earlier demonstrate that overgrown ($G > 20\ G_0$) junctions are stable in 1 mM pyridine in 1:1 MeOH−H_2O under ECP control with potentials in the range -1.2 V $\leq E_1 \leq +0.2$ V *vs* Ag/AgCl. Thus, the same potential range was chosen to explore the effect of applied potential on the chemical noise signatures of ASJs with adsorbed pyridine. Four potentials were chosen for detailed study: $E_1 = +0.2$, -0.2, -0.6 and -1.0 V. The characteristic frequencies corresponding to adsorption−desorption of 1 mM pyridine were determined by the fifth-order polynomial procedure developed previously,[34] and the f_c values and distributions are shown in Figures 8 and 9, respectively. Clearly, f_c increases as the applied

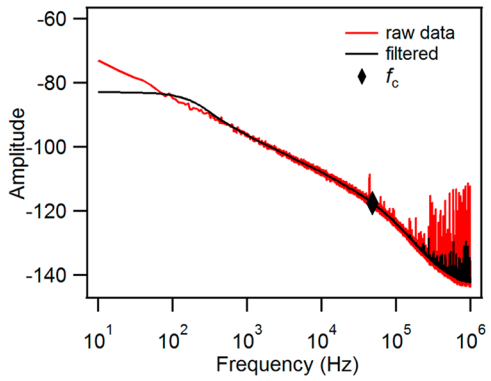

Figure 7. Typical power spectral density (PSD) of current measured in Au−Ag−Au ASJs in 1 mM pyridine. The presence of chemical noise changes the slope of the PSD at the cutoff frequency, f_c. PSDs are measured from raw (red) or filtered (black) data.

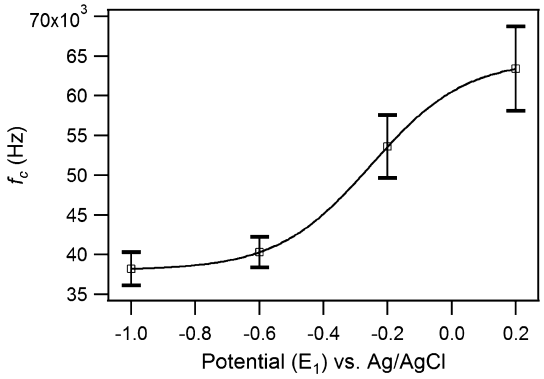

Figure 8. Cutoff frequency as a function of applied potential for 1 mM pyridine in 1:1 MeOH−H_2O at a Au−Ag−Au bimetallic ASJ under ECP control. Error bars represent ±2 times the standard deviation of the mean determined over 80 runs. The solid line is a fit to a sigmoidal function as a guide to the eye.

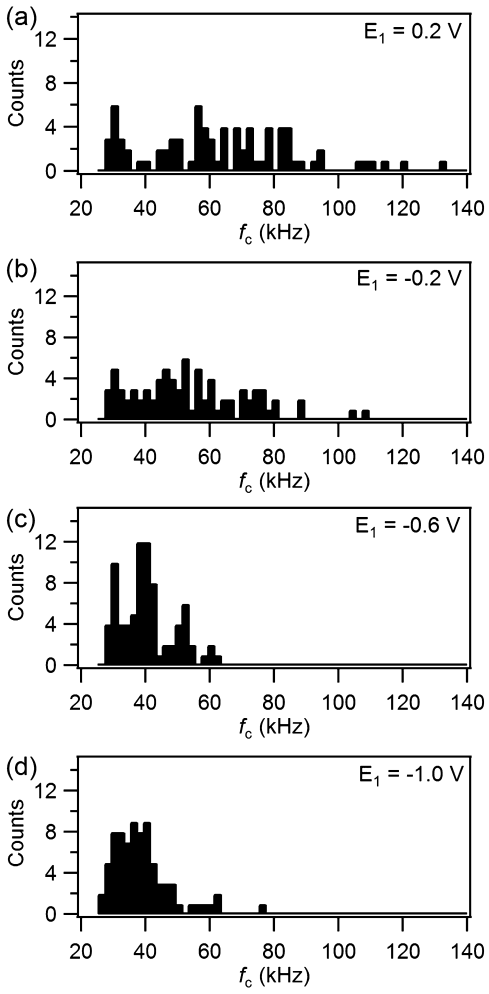

Figure 9. Distributions of f_c values determined from 80 runs at each of four different applied potentials for 1 mM pyridine in 1:1 MeOH−H_2O at an Au−Ag−Au bimetallic ASJ. (a) E_1 = +0.2 V, (b) E_1 = −0.2 V, (c) E_1 = −0.6 V, (d) E_1 = −1.0 V.

potential increases to the anodic side; however, the uncertainties in f_c increase at more anodic potentials. The f_c distributions as a function of applied ECP shown in Figure 9 are consistent with the uncertainties, as reflected in the standard deviations of the mean determined for the f_c values, shown in Figure 8. The distribution of f_c is broad and nearly uniform at the most anodic potential, E_1 = +0.2 V, Figure 9a, and becomes much sharper and peaked when the applied potential is shifted in the cathodic direction, *cf.* E_1 = −1.0 V, Figure 9d.

The simplest interpretation of surface adsorption−desorption posits a Langmuir model, in which the relaxation time, τ, is related to the adsorption and desorption kinetics by $1/\tau = k_a C_A + k_d$, where k_a and k_d are the rate constants for adsorption and desorption, respectively, and C_A is the adsorbate concentration. Changing the applied potential on a macroscopic electrode alters the surface charge density and can affect the adsorption−desorption kinetics, so $f_c = (2\pi\tau)^{-1}$ would vary as a function of ECP, as observed. Furthermore, in light of the behavior of overgrown junctions described above, the lability of ASJs increases as the potential is increased to more anodic values. All else being equal, increased lability should decrease τ and increase f_c going to more anodic potentials, as observed. However, these simple observations do not explain the wide variation of f_c distributions with potential.

One possibility is the local ECP, which varies spatially along the ASJ structure. The resistance of a 5 G_0 ASJ is ∼2.6 kΩ, which is comparable to the resistance of the ballast resistor, R_d in Figure 2. Under these conditions, the potentials dropped across the ASJ and the ballast resistor are comparable, and the ASJ experiences a reduced in-wire potential, $\Delta E - V_d$. However, reduction in voltage depends on the conductance of the ASJ and is to first-order independent of E_1. Therefore, varying local ECP is not likely to be responsible for the variation in f_c distributions with potential.

Another possibility ascribes the observed chemical noise to a more complex set of reactions than simple

adsorption and desorption of molecular pyridine. Additional reactions

$$Ag_{(s)} + C_6H_5N \underset{k_d}{\overset{k_a}{\rightleftarrows}} Ag\text{-}C_6H_5N_{(ads)} \quad (5)$$

$$Ag^+_{(solv)} + e^- \underset{k_{-1}}{\overset{k_1}{\rightleftarrows}} Ag_{(s)} \quad (6)$$

$$Ag\text{-}C_6H_5N^+_{(solv)} + e^- \underset{k_{-2}}{\overset{k_2}{\rightleftarrows}} Ag\text{-}C_6H_5N_{(ads)} \quad (7)$$

$$Ag(C_6H_5N)_2{}^+_{(solv)} + e^- \underset{k_{-3}}{\overset{k_3}{\rightleftarrows}} Ag(C_6H_5N)_{2(ads)} \quad (8)$$

would occur with their own characteristic relaxation kinetics and would no longer reflect simple kinetics. Surface-enhanced Raman spectroscopy (SERS) studies of the Ag–pyridine system exhibit evidence of Ag–pyridine complexes, $Ag(pyridine)^+$, and $Ag(pyridine)_2{}^+$ as an extra band in the SERS spectrum at 1025 cm^{-1} after anodic etching of Ag–pyridine surfaces[47] and as additional channels of signal enhancement.[48]

Consider the four reactions 5–8. When the ECP is cathodic, the oxidative desorption of Ag, Ag(pyridine), and $Ag(pyridine)_2$, as their respective monocations, is unlikely, because $k_1, k_2, k_3 \gg k_{-1}, k_{-2}, k_{-3}$. As a result, only reaction 5, pyridine adsorption–desorption, is appreciable, and the detected chemical noise is determined solely by that reaction. As the potential shifts to more anodic values, the additional oxidative reactions 6–8 would be expected to start to contribute to the observed dynamics. Furthermore, f_c has been shown to be concentration-dependent and, by the adsorption isotherm, coverage-dependent,[34] as is the ASJ lability. Thus, not only does desorption from an ASJ change surface coverage, it also changes the intrinsic restructuring dynamics of the ASJ itself, behavior that is likely reflected in the complex f_c distributions observed at anodic potentials. While it is not possible to compare the kinetics of pyridine adsorption–desorption at different ECPs, because different reactions contribute to the dynamics at anodic potentials, it is possible to compare f_c of ASJs at a very cathodic, and therefore intrinsically stable, potential of −1.0 V to that obtained with the ASJ floating, all other conditions being held the same. In 1 mM pyridine at $E_1 = -1.0$ V, $\langle f_c \rangle = 3.82 \times 10^4$ Hz, and when the ASJ is floating, $\langle f_c \rangle = 1.04 \times 10^5$ Hz. In both cases, the dynamics largely result from simple pyridine adsorption–desorption, but the large difference in $\langle f_c \rangle$ shows that k_a and k_d are strongly affected by the electrochemical potential.

CONCLUSIONS

Electrochemical potential clearly plays an important role in determining the dynamics of pyridine on Au–Ag–Au bimetallic ASJs. First, overgrown ($G > 20\ G_0$) Ag nanojunctions exhibit electrochemical potential-dependent stability. Three different classes of conductance behavior are observed, which can be explained by the interplay of several factors. Ag oxidation is obviously important at anodic potentials, with the onset of the process being determined by the size of the Ag junction and the nature of the surrounding material. ECP-induced surface stress can also result in conductance changes. Finally, the presence of certain adsorbates, *e.g.*, pyridine, stabilizes the junction by lowering the surface energy and protecting Ag from solvent-mediated corrosion. On the other hand, when Au–Ag–Au ASJs are held at cathodic potentials, the junction can be very stable over extended periods.

Electrochemical potential also influences the dynamics of molecular adsorption–desorption, as reflected in the chemical noise contribution to the power spectral density. Fluctuations in the population of surface pyridine, detected through the presence of Lorentzian components in the relaxation frequency spectrum, reveal the kinetics of adsorption–desorption through a characteristic cutoff frequency, f_c. Changing the electrochemical potential of the ASJ alters f_c, with higher frequencies being observed at more anodic potentials, an observation consistent with a number of oxidative desorption processes being turned on at anodic potentials. Multiple surface reactions, characterized by the desorption of species $Ag(pyridine)_n$, $0 \le n \le 2$, are affected by the applied potential, resulting in substantial changes in the chemical noise signature.

The use of ECP to control the fabrication and behavior of ASJs holds significant promise. Coupling fluctuation spectroscopy to mesoscopic molecular assemblies supported on ASJs can reveal chemical noise that carries both analytical (concentration) and dynamic (kinetics) information. Future studies will target other materials, such as Pt, with more anodic redox potentials to further explore the relationship among nanowire restructuring dynamics, surface molecular fluctuations, and electrochemical potential.

EXPERIMENTAL SECTION

Sample Preparation. Templates are fabricated by microfabrication, the details of which have been described previously.[33] Briefly, a 100 nm Au microbridge, *ca.* 6 μm wide × 20 μm long, is defined on a SiO_2/Si wafer using standard photolithography and lift-off techniques. Then a 100 nm layer of SiN_x is deposited by plasma-enhanced chemical vapor deposition as an insulating layer. A Cr mask is then deposited, and reactive ion etching is used to expose Au contact pads. The Cr layer is then removed with Cr etchant. In the final step focused ion beam milling is used to create a tip-and-anvil electrode configuration with ≤100 nm separation, as shown in Figure 1b. A fluidic channel (1 mm × 500 μm) made with polydimethylsiloxane (PDMS) is then aligned to and sealed on the template. One end

of the channel is connected to a syringe pump for solution delivery, and the other end is left open to contain a Ag/AgCl counter/reference electrode, Figure 1d.

Ag ASJ Formation. Ag ASJs are formed between the gap of two Au electrodes by potential-controlled electroplating in an electrolyte solution containing 10 μM Ag_2SO_4 and 0.1 M K_2SO_4 using a commercial potentiostat (Gamry Instruments, Reference 600). This approach initially generates overgrown junctions ($G \gg 1\ G_0$). Once the junction is formed, the electroplating solution is then removed and replaced with pyridine solution (1 mM or 1 μM pyridine in 1:1 (v:v) H_2O−MeOH) to prevent self-thinning by Ag dissolution in the Ag^+-containing electrolyte solution and/or Ag oxidation. Different flow rates are used in different parts of the experiment. To reduce self-thinning of the overgrown junction, the flow rate is set to 2−3 mL h^{-1} during junction growth. After the solution is switched, the flow rate is reduced to 0.05 mL h^{-1} to minimzie mechanical disturbance from fluidic flow. The fabrication of ASJs for chemical noise measurements is initiated by ECP-induced oxidation at the early, thick-junction stage followed by current-induced electromigration when the junction is close to atomic size, $G < 20\ G_0$, the latter process being controlled by an adjustable resistor in series with the sample. Ag junctions were regrown to form a fresh Ag surface for each run.

Conductance Measurements under ECP Control. Following deposition of an overgrown junction, pyridine solution is admitted to the flow cell, and potential control is established, as shown in Figure 2. The voltage source is the analog output of a data acquisition (DAQ) card (National Instrument, PCIe-6361) that exhibits low intrinsic electronic noise. Conductance measurements are performed by measuring the potential drop across the ballast resistor (R_d), using the analog input of the DAQ card. A customized Labview program converts the measured voltage data into conductance values and calculates the PSD in real time, allowing both the conductance and the frequency spectrum to be monitored at the same time. Conductance measurements are made at 10 Hz, and noise measurements are made at 2 MHz. Each single frequency spectrum is constructed using 0.1 s of data (200 000 samples), and typically, 100 spectra (10 s) averaged in Labview constitute a single run.

Conflict of Interest: The authors declare no competing financial interest.

Acknowledgment. This work was supported by the National Science Foundation through grant 1111739. The authors thank H. White for useful discussions.

REFERENCES AND NOTES

1. Brandbyge, M.; Sorensen, M. R.; Jacobsen, K. W. Conductance Eigenchannels in Nanocontacts. *Phys. Rev. B* **1997**, *56*, 14956–14959.
2. CostaKramer, J. L.; Garcia, N.; GarciaMochales, P.; Serena, P. A.; Marques, M. I.; Correia, A. Conductance Quantization in Nanowires Formed between Micro and Macroscopic Metallic Electrodes. *Phys. Rev. B* **1997**, *55*, 5416–5424.
3. Cuevas, J. C.; Yeyati, A. L.; Martín-Rodero, A. Microscopic Origin of Conducting Channels in Metallic Atomic-Size Contacts. *Phys. Rev. Lett.* **1998**, *80*, 1066–1069.
4. van Ruitenbeek, J. M.; Devoret, M. H.; Esteve, D.; Urbina, C. Conductance Quantization in Metals: The Influence of Subband Formation on the Relative Stability of Specific Contact Diameters. *Phys. Rev. B* **1997**, *56*, 12566–12572.
5. Li, C. Z.; He, H. X.; Bogozi, A.; Bunch, J. S.; Tao, N. J. Molecular Detection Based on Conductance Quantization of Nanowires. *Appl. Phys. Lett.* **2000**, *76*, 1333–1335.
6. Castle, P. J.; Bohn, P. W. Interfacial Scattering at Electrochemically Fabricated Atom-Scale Junctions between Thin Gold Film Electrodes in a Microfluidic Channel. *Analyt. Chem.* **2005**, *77*, 243–249.
7. Bogozi, A.; Lam, O.; He, H. X.; Li, C. Z.; Tao, N. J.; Nagahara, L. A.; Amlani, I.; Tsui, R. Molecular Adsorption onto Metallic Quantum Wires. *J. Am. Chem. Soc.* **2001**, *123*, 4585–4590.
8. Agrait, N.; Yeyati, A. L.; van Ruitenbeek, J. M. Quantum Properties of Atomic-Sized Conductors. *Phys. Rep.* **2003**, *377*, 81–279.
9. Tsutsui, M.; Shoji, K.; Taniguchi, M.; Kawai, T. Formation and Self-Breaking Mechanism of Stable Atom-Sized Junctions. *Nano Lett.* **2008**, *8*, 345–349.
10. Xu, B. Q.; Tao, N. J. J. Measurement of Single-Molecule Resistance by Repeated Formation of Molecular Junctions. *Science* **2003**, *301*, 1221–1223.
11. Shi, P.; Bohn, P. W. Stable Atom-Scale Junctions on Silicon Fabricated by Kinetically Controlled Electrochemical Deposition and Dissolution. *ACS Nano* **2008**, *2*, 1581–1588.
12. Xie, F. Q.; Huser, F.; Pauly, F.; Obermair, C.; Schon, G.; Schimmel, T. Conductance of Atomic-Scale Pb Contacts in an Electrochemical Environment. *Phys. Rev. B* **2010**, 82.
13. Boussaad, S.; Tao, N. J. Atom-Size Gaps and Contacts between Electrodes Fabricated with a Self-Terminated Electrochemical Method. *Appl. Phys. Lett.* **2002**, *80*, 2398–2400.
14. Popa, P. L.; Dalmas, G.; Faramarzi, V.; Dayen, J. F.; Majjad, H.; Kemp, N. T.; Doudin, B. Heteronanojunctions with Atomic Size Control Using a Lab-on-Chip Electrochemical Approach with Integrated Microfluidics. *Nanotechnology* **2011**, 22.
15. Lu, W.; Jeong, D. S.; Kozicki, M.; Waser, R. Electrochemical Metallization Cells-Blending Nanoionics into Nanoelectronics? *MRS Bull* **2012**, *37*, 124–130.
16. Natelson, D.; Di Ventra, M. Ion Motion and Electrochemistry in Nanostructures. *MRS Bull.* **2011**, *36*, 914–920.
17. Valov, I.; Sapezanskaia, I.; Nayak, A.; Tsuruoka, T.; Bredow, T.; Hasegawa, T.; Staikov, G.; Aono, M.; Waser, R. Atomically Controlled Electrochemical Nucleation at Superionic Solid Electrolyte Surfaces. *Nat. Mater.* **2012**, *11*, 530–535.
18. Valov, I.; Waser, R.; Jameson, J. R.; Kozicki, M. N. Electrochemical Metallization Memories-Fundamentals, Applications, Prospects. *Nanotechnology* **2011**, 22.
19. Waser, R.; Dittmann, R.; Staikov, G.; Szot, K. Redox-Based Resistive Switching Memories - Nanoionic Mechanisms, Prospects, and Challenges. *Adv. Mater.* **2009**, *21*, 2632.
20. Schirm, C.; Matt, M.; Pauly, F.; Cuevas, J. C.; Nielaba, P.; Scheer, E. A Current-Driven Single-Atom Memory. *Nat. Nanotechnol.* **2013**, *8*, 645–648.
21. Shu, C.; Li, C. Z.; He, H. X.; Bogozi, A.; Bunch, J. S.; Tao, N. J. Fractional Conductance Quantization in Metallic Nanoconstrictions under Electrochemical Potential Control. *Phys. Rev. Lett.* **2000**, *84*, 5196–5199.
22. Manabu, K.; Kei, M. Metal Atomic Contact under Electrochemical Potential Control. *J. Phys.: Condens. Matter* **2012**, *24*, 164212.
23. Kiguchi, M.; Konishi, T.; Miura, S.; Murakoshi, K. The Effect of Hydrogen Evolution Reaction on Conductance Quantization of Au, Ag, Cu Nanocontacts. *Nanotechnology* **2007**, *18*, 424011.
24. Konishi, T.; Kiguchi, M.; Murakoshi, K. Electrical Conductance of Rh Atomic Contacts under Electrochemical Potential Control. *Phys. Rev. B* **2010**, *81*, 125422.
25. Xu, B. Q.; He, H. X.; Tao, N. J. Controlling the Conductance of Atomically Thin Metal Wires with Electrochemical Potential. *J. Am. Chem. Soc.* **2002**, *124*, 13568–13575.
26. Shi, P.; Bohn, P. W. Electrochemical Control of Stability and Restructuring Dynamics in Au-Ag-Au and Au-Cu-Au Bimetallic Atom-Scale Junctions. *ACS Nano* **2010**, *4*, 2946–2954.
27. Li, J.; Nakato, Y.; Murakoshi, K. Electrochemical Fabrication of Pd-Au Heterogeneous Nanocontact Showing Stable Conductance Quantization under Applying High Bias Voltage. *Chem. Lett.* **2005**, *34*, 374–375.
28. Xie, F. Q.; Maul, R.; Augenstein, A.; Obermair, C.; Starikov, E. B.; Schön, G.; Schimmel, T.; Wenzel, W. Independently Switchable Atomic Quantum Transistors by Reversible Contact Reconstruction. *Nano Lett.* **2008**, *8*, 4493–4497.
29. Zhang, Y. M.; Terrill, R. H.; Bohn, P. W. Chemisorption and Chemical Reaction Effects on the Resistivity of Ultrathin Gold Films at the Liquid-Solid Interface. *Analyt. Chem.* **1999**, *71*, 119–125.
30. He, H. X.; Shu, C.; Li, C. Z.; Tao, N. J. Adsorbate Effect on the Mechanical Stability of Atomically Thin Metallic Wires. *J. Electroanal. Chem.* **2002**, *522*, 26–32.

31. Kiguchi, M.; Miura, S.; Murakoshi, K. Fabrication of Stable Metal Nanowire Showing Conductance Quantization in Solution. *Surf. Sci.* **2007**, *601*, 4127–4130.
32. Leroux, Y. R.; Fave, C.; Zigah, D.; Trippe-Allard, G.; Lacroix, J. C. Atomic Contacts *via* Electrochemistry in Water/Cyclodextrin Media: A Step toward Protected Atomic Contacts. *J. Am. Chem. Soc.* **2008**, *130*, 13465–13470.
33. Hwang, T.-W.; Bohn, P. W. Robust Au−Ag−Au Bimetallic Atom-Scale Junctions Fabricated by Self-Limited Ag Electrodeposition at Au Nanogaps. *ACS Nano* **2011**, *5*, 8434–8441.
34. Hwang, T.-W.; Branagan, S. P.; Bohn, P. W. Chemical Noise Produced by Equilibrium Adsorption/Desorption of Surface Pyridine at Au−Ag−Au Bimetallic Atom-Scale Junctions Studied by Fluctuation Spectroscopy. *J. Am. Chem. Soc.* **2013**, *135*, 4522–4528.
35. Green, M.; Liu, F. M. Sers Substrates Fabricated by Island Lithography: The Silver/Pyridine System. *J. Phys. Chem. B* **2003**, *107*, 13015–13021.
36. Plieth, W. J. Electrochemical Properties of Small Clusters of Metal Atoms and Their Role in the Surface Enhanced Raman Scattering. *J. Phys. Chem.* **1982**, *86*, 3166–3170.
37. Redmond, P. L.; Hallock, A. J.; Brus, L. E. Electrochemical Ostwald Ripening of Colloidal Ag Particles on Conductive Substrates. *Nano Lett.* **2004**, *5*, 131–135.
38. Ivanova, O. S.; Zamborini, F. P. Size-Dependent Electrochemical Oxidation of Silver Nanoparticles. *J. Am. Chem. Soc.* **2009**, *132*, 70–72.
39. Bach, C. E.; Giesen, M.; Ibach, H.; Einstein, T. L. Stress Relief in Reconstruction. *Phys. Rev. Lett.* **1997**, *78*, 4225–4228.
40. Brunt, T. A.; Chabala, E. D.; Rayment, T.; O'Shea, S. J.; Welland, M. E. Measuring Surface Stress Induced by Electrode Processes Using a Micromechanical Sensor. *J. Chem. Soc., Faraday Trans.* **1996**, *92*, 3807–3812.
41. Xu, He; Tao, N. J. Controlling the Conductance of Atomically Thin Metal Wires with Electrochemical Potential. *J. Am. Chem. Soc.* **2002**, *124*, 13568–13575.
42. Rubio, G.; Agraït, N.; Vieira, S. Atomic-Sized Metallic Contacts: Mechanical Properties and Electronic Transport. *Phys. Rev. Lett.* **1996**, *76*, 2302–2305.
43. Somorjai, G. A.; Van Hove, M. A. Adsorbate-Induced Restructuring of Surfaces. *Prog. Surf. Sci.* **1989**, *30*, 201–231.
44. He, Y.; Borguet, E. Effect of Local Environment on Nanoscale Dynamics at Electrochemical Interfaces: Anisotropic Growth and Dissolution in the Presence of a Step Providing Evidence for a Schwoebel-Ehrlich Barrier at Solid/Liquid Interfaces. *Faraday Discuss.* **2002**, *121*, 17–25.
45. Haftel, M. I.; Einstein, T. L. Influence of the Electrochemical Potential on Energy Landscapes near Step- and Island-Edges: Ag(100) and Ag(111). *Appl. Surf. Sci.* **2001**, *175−176*, 49–54.
46. Feher, G.; Weissman, M. Fluctuation Spectroscopy - Determination of Chemical Reaction-Kinetics from Frequency Spectrum of Fluctuations. *Proc. Natl. Acad. Sci. U.S.A.* **1973**, *70*, 870–875.
47. Potapkina, E. V.; Denisova, A. S.; Myund, L. A.; Makarov, A. A.; Dem'yanchuk, E. M. Investigation of Pyridine−Ag(X), Aqueous Solutions: Sers and Raman Study Supported by NMR Spectroscopy. *J. Mol. Struct.* **2011**, *996*, 128–134.
48. Watanabe, T.; Kawanami, O.; Honda, K.; Pettinger, B. Evidence for Surface Ag+ Complexes as the Sers-Active Sites on Ag Electrodes. *Chem. Phys. Lett.* **1983**, *102*, 565–570.